The effect of compaction on the mechanical behaviour of mix granulate base course materials and on pavement performance

A.A. van Niekerk and J. van Scheers
Delft University of Technology, Road and Railroad Research Laboratory, The Netherlands

P. Muraya and A. Kisimbi
M.Sc. graduate students, IHE Delft, The Netherlands

The results of large scale triaxial tests (d x h=300*600 mm) as performed on a specific mix granulate compacted to four degrees of compaction (D.o.C.) are presented in terms of measured and modelled failure, resilient and permanent deformation behaviour. In addition finite element design calculations have been conducted on the basis of the measured mechanical behaviour to demonstrate the influence of the D.o.C. of the base course layer on the performance of different pavements. Thus in addition to the conventional design criteria of asphalt and subgrade strain (fatigue cracking and permanent subgrade deformation), safety against base shear failure and permanent deformation in the base course and sub-base layers, resulting in rutting at the pavement surface, have also been considered.
The results clearly demonstrate the importance of adequate base course compaction on pavement performance and of considering design criteria for the base course and sub-base especially when dealing with pavements in which an important structural contribution is required from the base course and sub-base (thinner toplayers and small-element pavements). In such pavements stresses in the base should be limited to prevent base failure and to limit permanent deformation under repeated loading.

Keywords: **mechanical behaviour, granular base course materials, compaction, triaxial testing**

1 Introduction

In this paper the influence of compaction on the mechanical behaviour of a granular base course material (mix granulate) and on the resulting performance of pavements is described.
The paper describes the results of triaxial tests performed to establish the failure, resilient and permanent deformation behaviour of an especially composed mix granulate compacted to 97%, 100%, 103% and 105% of maximum Proctor density. Various stress dependent models have been applied to model the observed behaviour.
By means of finite element calculations in which the modelled material behaviour has been incorporated, the performance of a 50 mm and a 100 mm asphaltic pavement and of a 80 mm concrete block (CB) pavement has been analysed. For these three pavements only the degree of compaction

(D.o.C.) of the base course (thus resulting in different mechanical behaviour) has been taken as a design variable.
The performance of these 12 "pavements" (3 types x 4 D.o.C.) has been analysed not only on the basis of the "conventional" design criteria of asphalt and subgrade strain but also on the basis of stability (shear failure) and permanent deformation of the granular base and sub-base layers.

2 Tested materials

Mix granulates, i.e. mixes of granulated concrete rubble and masonry rubble processed from demolition waste, are the most extensively used unbound/lightly bound granular base course materials in the Netherlands. For the specifications relating to the grading, composition and mechanical properties of mix granulates reference is made to [Niekerk et al., 2000].
For this research large quantities of concrete and masonry granulate crushed by a jaw and an impact crusher have been sieved in the following fractions: < 0.250 mm, 0.250-0.5 mm, 0.5-1.0 mm, 1-2 mm, 2-4 mm, 4-8 mm, 8-16 mm, 16-31.5 mm, 31.5-45 mm were available. From these fractions it was thus possible to compose mix granulates to all possible gradings and compositions (the amount of concrete to masonry granulate). For the tests described in this paper an "average" mix granulate (AL-40) has been composed out of the above described fractions. AL-40 represents an average with respect to:

- *grading*: in Figure 1 grading AL-40 (average limits) represents the average between the upper (UL-40) and the lower (LL-40) limit of the grading envelope prescribed in the Netherlands for a 0/40 mm granular base material
- *composition*: 65% [by mass] of concrete granulate, i.e. between 50% and 80%. According to the Dutch standards a mix granulate should consist of at least 50% and at most 80% [by mass] of concrete granulate. The complement consists mainly of crushed masonry and a limited, prescribed amount of impurities (glass, wood, gypsum, etc.).

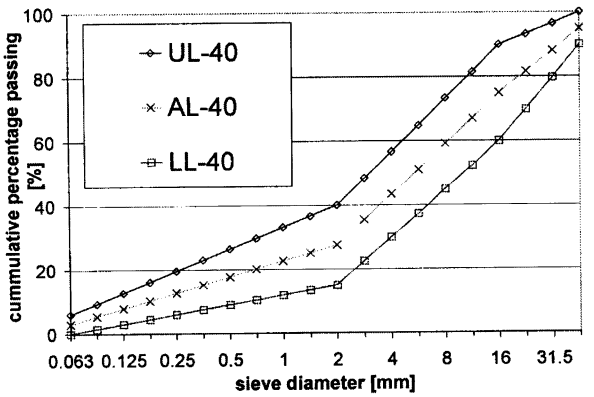

Figure 1: Particle size distribution curve for AL-40 in relation to grading envelope.

To obtain a reference density for the AL-40 mix granulate, a density-moisture relation at 4 increasing moisture contents (6, 8, 10 and 12 % [by mass]) has been established using the Dutch specifications for the Proctor test [Niekerk et al., 2000].

As the dry density-moisture relation was found to be rather flat, without showing a distinctive optimum moisture content, the "Proctor" density has been calculated for AL-40 as the average of the found dry densities (i.e.: 1735 kg/m^3) at the 4 moisture contents.

3 Triaxial test results

3.1 *Introduction*

In this section the results of the triaxial failure, resilient and permanent deformation tests performed on AL-40 compacted to different degrees of compaction (97%, 100% and 103% MPD) are presented in terms of measured and modelled behaviour.

At first very briefly some aspects related to the performed triaxial tests will be given. For more details relating to specimen preparation, test execution and data interpretation reference is made to the first paper by the same authors in these proceedings [Niekerk et al., 2000].

Given the coarse grading of mix granulates the triaxial tests have been performed in a large scale triaxial facility on specimens with a diameter of 300 mm and a height of 600 mm (specimen volume 0.045 m^3 and specimen mass 80 – 100 kg).

In this facility the application of loads and stresses is effectuated by:

- an hydraulic actuator and a closed loop feedback control system, capable of applying an accurately controlled vertical monotonic or cyclic (haversine shaped) loading upto 150 kN at a frequency up to 5 Hz.
- (partial) internal vacuum, for applying the confining stress. This thus implies that the test can only be conducted as a constant confining pressure (CCP) test. By the difference between the ambient air pressure and the partial internal vacuum a confining pressure can be applied between 0 and 90 kPa.

Although a CCP test is not as good a simulation of the stresses occurring in a pavement under traffic loading as a variable confining pressure (VCP) test it is at present at these large specimen sizes more feasible for practice than a VCP test.

To be able to apply confinement to a specimen during the test it has to be contained in an air tight membrane. The specimen is compacted in a split-mould, in which a first membrane is placed. After compaction (in 6 layers) and sealing of the membrane to the top plate, the specimen is placed under an internal (partial) vacuum and released from the splitmould. As the first membrane is often partially punctured, a second membrane is placed over the specimen, sealing it completely air-tight.

The axial and radial deformations, resulting from loading of the specimen under different stress combinations in either the resilient or the permanent deformation tests, are measured by means of on sample LVDT-s. For this two sets of three small blocks are glued to the outer membrane at 1/3 and 2/3 of the specimen height respectively. On these blocks two self-centring rings are laid which serve as a local reference for the 3 axial and the 2 sets of 3 radial LVDT-s, see Figure 2. Two sets of LVDT-s with different measuring ranges are used:

- resilient deformations are measured with LVDT-s with a total measuring range of 1 mm over 20 V output range,
- permanent deformations are measured with LVDT-s with a total measuring range of 20 mm over 20 V output range.

For establishing the stress dependent mechanical behaviour three different types of triaxial tests have been performed:

- cyclic loading resilient deformation tests,
- cyclic loading permanent deformation tests,
- monotonic loading failure tests.

Granular materials exhibit stress dependent (i.e.: non-linear) mechanical behaviour. To therefore determine the mechanical behaviour (strength, stiffness and resistance to permanent deformation) tests have to be performed at different stress levels (magnitudes) and different stress combinations (deviatoric stress to confining stress). It is often assumed that if a granular material is loaded in its "elastic" range (small strains) for a limited number of load repetitions the loading history does not affect its response. The response under multiple stress levels and stress combinations can then be determined on one and the same specimen (resilient deformation test).

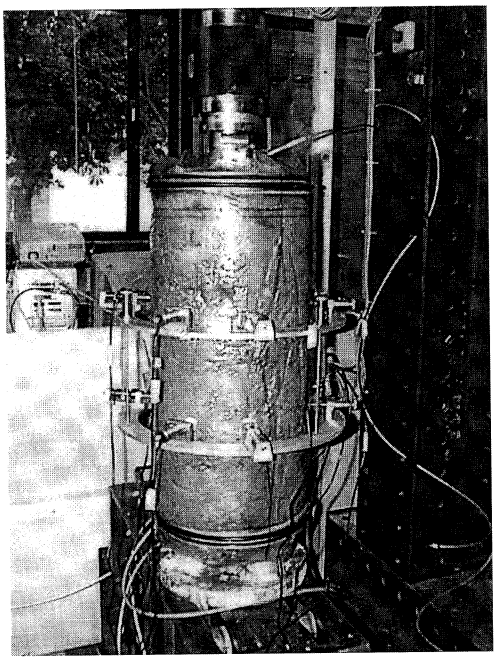

Figure 2: Finished and instrumented triaxial specimen.

If a specimen is however loaded beyond its "elastic" range (small strains) or for a very large amount of load repetitions (N) the loading history does affect its response. For this reason permanent deformation tests, in which the accumulation of strain upto $N=10^6$, are determined on "virgin" specimens for each new stress level.

3.2 *Resilient deformation tests*

In a so called M_r-θ test for determination of the stress dependent resilient deformation behaviour a specimen is subjected to a large number of deviator stress to confining stress ratio's (σ_c/σ_3 = 2,3,4,…,8) at different σ_3-levels (σ_3 = 12, 24, 36, 48, 60 and 72 kPa).
At each σ_c/σ_3 -ratio the specimen is subjected to 50 load repetitions. At the 50th load repetition the data acquisition system captures and records full force, stress and deformation signals.
In Figure 3 the stresses applied in the triaxial test are summarised.

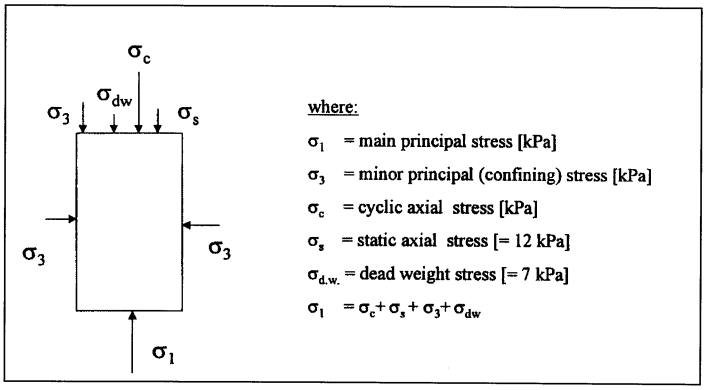

Figure 3: Stresses applied in triaxial test.

From the measured deformations the resilient axial ($\varepsilon_{ax,\,res}$) and radial strains ($\varepsilon_{rad,\,res}$) are calculated as the measured axial or radial deformation divided by respectively the measuring length (200 mm) or the specimen radius (150 mm).
From the applied stresses and the resulting resilient strains the resilient properties (e.g. resilient modulus, M_r and Poisson's ratio, v) can be determined according to:

$$M_r = \frac{\sigma_c}{\varepsilon_{ax,res}} \quad (1); \qquad v = -\frac{\varepsilon_{rad,res}}{\varepsilon_{ax,\,res}} \quad (2)$$

The stress dependency as observed for M_r and v from these tests has been modelled by means of 2 models for M_r and 2 models for v by means of non-linear multi-variable regression analysis.
For M_r the well known M_r-θ - model [Brown and Pell, 1967] and the more universal M_r - σ_3 - σ_d - model [Uzan et al., 1992] have been fitted:

$$M_r = k_1\left(\frac{\theta}{\theta_0}\right)^{k_2} \quad (3); \qquad M_r = k_1\left(\frac{\sigma_3}{\sigma_{3,0}}\right)^{k_2}\left(\frac{\sigma_d}{\sigma_{d,o}}\right)^{k_3} \quad (4)$$

where:

θ	:	sum of principal stresses [kPa]
		$\theta = \sigma_1 + 2\,\sigma_3 = \sigma_c + \sigma_s + 3\sigma_3 + \sigma_{d.w.}$
σ_3	:	minor principal stress [kPa]
σ_d	:	deviator stress (σ_1 - σ_3) [kPa]
θ_0, $\sigma_{3,0}$,$\sigma_{d,0}$	:	reference values (= 1 kPa)
k_1	:	regression coefficient [MPa]
k_2, k_3	:	regression coefficients [-]

The stress dependency of ν was found to be very well explained by the σ_1/σ_3-ratio and by σ_3 according to the following two models [Huurman, 1997]:

$$\nu = a\left(\frac{\sigma_1}{\sigma_3}\right)^b \quad (5); \qquad \nu = a\left(\frac{\sigma_1}{\sigma_3}\right)^b \left(\frac{\sigma_3}{\sigma_{3,0}}\right)^c \quad (6)$$

where σ_1 is defined in Figure 3 and *a, b, c* are regression coefficients [-].

Figure 4 shows a plot of the measured M_r-values plotted against θ, the sum of the principal stresses. In this plot also the M_r-θ model (equation 3) is given. It can be seen that this model describes the data reasonably but fails to discriminate between the influence of the different stress invariants (σ_3 and $\sigma_d = \sigma_1 - \sigma_3$). The legend to Figure 4 shows the M_r–values at the different σ_3 –values with different symbols. With respect to the influence of σ_3 and σ_d it can be observed that:

- M_r-values increase (slightly) with σ_3 increasing from 12 to 72 kPa.
- At a given σ_3 value M_r at first increases with increasing σ_d/σ_3 – values and then stabilises or even decreases as the σ_d/σ_3 -value increases further.

This observed behaviour can be better described by the M_r - σ_3 - σ_d – model (equation 4), although this model is not capable of describing both the initial increase of M_r followed by the subsequent decrease of M_r with increasing σ_d/σ_3 – values.

In Figure 4 this decrease of M_r at increasing σ_d/σ_3 –ratios is observed for all σ_3 – levels, except 12 and 72 kPa. At these higher σ_d/σ_3 –levels the specimen experiences a bit of permanent deformation over the 50 load repetitions which are applied up to the measurement, indicating that the material is stressed beyond its elastic range. For this reason the loading is then stopped at that specific σ_3 – level and taken to the next higher σ_3 –level.

In this research 4 M_r-θ tests have been conducted on 4 different specimens at 4 target D.o.C., the specimens for the tests at the different D.o.C. have all been prepared at a target moisture content of 8% [m/m]. Table 1 gives the actually achieved D.o.C. and moisture contents.

Table 2 and Table 3 give the regression coefficients of the 4 models fitted for M_r and ν. The high r^2-values indicate good fits between the data and the models. It has to be remarked that the fit of these models would be a bit poorer if the tests had been extended to higher σ_d/σ_3 –ratios.

Figure 5 gives the M_r-θ models as found for the different D.o.C., it clearly demonstrates the influence of the D.o.C. on M_r. As the D.o.C. increases from 97.3% to 105.2% the M_r-values increase from 130 to 260 MPa for θ-values of 100 kPa and from 285 to 570 MPa for θ-values of 800 kPa.

Table 1. Desired and achieved D.o.C. and moisture contents for the M_r-θ test specimens

Desired D.o.C.	wet density	MC	Achieved D.o.C.
[%]	[kg/m^3]	[% m/m]	[%]
97	1833	8.52	97.3
100	1873	7.76	100.2
103	1931	8.29	102.8
105	1983	8.63	105.2

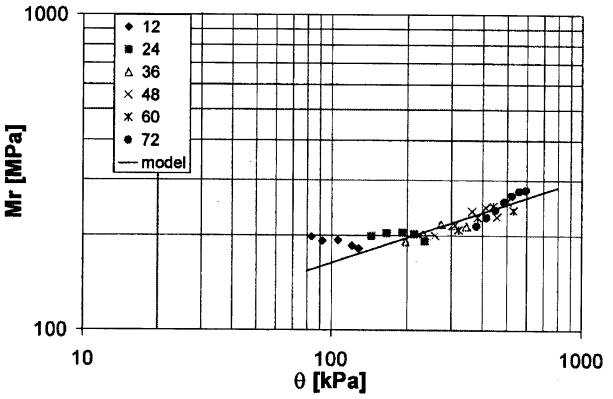

Figure 4. M_r-θ plot (data and model) for AL-40 at a D.o.C. of 97.3%.

Table 2. k_1, k_2, k_3 and r^2 – values for the fitted M_r-θ and M_r - σ_3 - σ_d - models

	k_1	k_2	k_3	r^2
	[MPa]	[-]	[-]	[-]
97	48.1	0.266		0.799
	64.7	0.091	0.171	0.820
100	14.9	0.465		0.845
	26.9	0.227	0.236	0.854
103	26.9	0.439		0.985
	45.7	0.119	0.297	0.987
105	43.5	0.385		0.970
	69.8	0.077	0.279	0.987
average:		M_r-θ		0.900
		M_r-σ_3-σ_d		0.912

Table 3. *a, b, c and* r^2 – values for the fitted v - σ_1/σ_3 and v-σ_1/σ_3 -σ_3 models

	a	*b*	*c*	r^2
	[-]	[-]	[-]	[-]
97	0.302	0.542		0.852
	0.225	0.570	0.064	0.880
100	0.241	0.595		0.808
	0.269	0.578	-0.021	0.811
103	0.214	0.646		0.969
	0.162	0.653	0.071	0.985
105	0.182	0.732		0.967
	0.133	0.738	0.079	0.986
average:		v -σ_1/σ_3		0.899
		n -σ_1/σ_3-σ_3		0.915

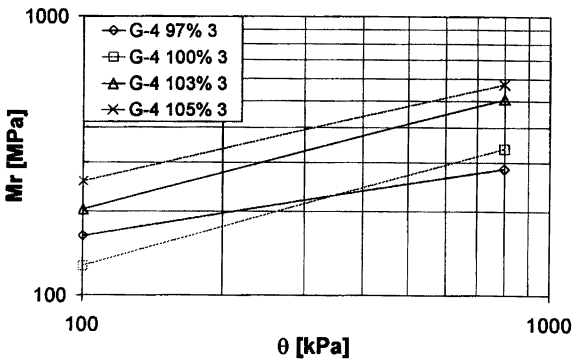

Figure 5: M_r-θ models for AL-40 at a D.o.C. of 97.3%, 100.2%, 102.8% and 105.2%

3.3 *Failure tests*

The magnitude of stress to which a granular material is subjected in relation to its maximum failure stress, has been found to greatly influence its response in terms of both resilient and permanent strains [Huurman, 1997].

The failure behaviour of granular materials is often characterised by the Mohr-Coulomb failure parameters c (cohesion) and ϕ (angle of internal friction). In terms of principal stresses the maximum major principal stress ($\sigma_{1,f}$) is determined by c, ϕ and the minor principal or confining stress (σ_3), according to equation 7 below (Mohr-Coulomb failure criterion, expressed in principal stresses):

$$\sigma_{1,f} = \frac{(1+\sin\phi)\cdot\sigma_3 + 2\cdot c\cdot\cos\phi}{(1-\sin\phi)} \qquad (7)$$

The failure tests have been performed in a displacement controlled mode (strain rate of 0.167%/s). In such a failure test a specimen is loaded under a monotonically increasing vertical stress (σ_1) upto failure at a constant σ_3. By determining the $\sigma_{1,f}$-values at a minimum of 3 different σ_3-levels (e.g. 12, 36 and 72 kPa) in these experiments, c and ϕ can determined by means of linear regression analysis. Table 4 gives the found values for c and ϕ for AL-40 at the different D.o.C. and for a sub-base sand which will be included in the FE-analysis in section 4.

The tests at the different increasing σ_3-levels have been performed as so called multi-stage tests (MST). In a MST the failure tests at the different σ_3-levels are performed on one and the same specimen rather then on three different specimens (single stage test). From earlier research [Kisimbi et al., 1999] it has been found that for granular materials MST results are very much comparable to the conventional SST results provided that the loading of the specimen is stopped when the maximum failure stress is reached, so as to limit excessive straining. This is ensured by closed loop feedback testing on the load signal.

Table 4. Cohesion and internal friction angles for sub-base sand and AL-40 at a D.o.C. of 97%, 100%, 103% (rounded values)

	D.o.C.	c	ϕ
	[%]	[kPa]	[°]
Sub-base	100	4.08	43.9
Base (AL-40)	97	55.5	36.9
	100	98.1	40.5
	103	89.5	42.9
	105	142.3	43.8

3.4 *Permanent deformation tests*

As discussed each *permanent* deformation (ε_p) test at a different stress ratio has to be performed on a new, "virgin" specimen. To establish the stress dependency of the permanent deformation behaviour for each D.o.C. at least 3 specimens have been tested in a ε_p- test. These 3 ε_p- tests have been performed at one constant σ_3–value of 12 kPa for 3 increasing σ_d/σ –ratios. In a ε_p- test the specimen is loaded cyclically (continuous haver-sine at a frequency of 5 Hz) upto either 10^6 load repetitions or the test is stopped when the specimen experiences some 10% permanent axial strain over the middle 1/3 part of the specimen (10% of 200mm). Throughout the test axial and radial on-sample deformations have been measured and recorded at designated load cycles (N=100, 200, ..., 1000, 2000, ..., 10000, 20000, ..., 100000, 200000, ..., 1000000).

Figure 6, Figure 7 and Figure 8 show the results of the 3 sets of 3 ε_p-tests performed on AL-40 at the D.o.C. of 97%, 100% and 103% of MPD, at present the ε_p-tests at D.o.C. = 105% have not yet been completed. In these figures the cumulative axial permanent strains are plotted against the number of load repetitions (N), both on logarithmic scales. In each figure at least 3 sets of points represent the measured strains at the different σ_d/σ_3–ratios. This ratio has however been expressed as the $\sigma_1/\sigma_{1,f}$ –ratio, which expresses how close the specimen is loaded to failure, according to the Mohr-Coulomb failure criterion. Similar plots can be made for the cumulative radial permanent strains, these are not given here.

The lines given in Figure 6, Figure 7 and Figure 8 represent the model lines which have been fitted to describe the observed behaviour. Equation 8 below gives the formulation of the fitted permanent deformation model [Huurman, 1997]. From equation 8 it can be observed that the model describes the dependency of the permanent strain (ε_p) with the number of load repetitions (N) in a stress dependent way ($\sigma_1/\sigma_{1,f}$-ratio, equations 8a to 8d).

$$\varepsilon_P = A \cdot \left(\frac{N}{1000}\right)^B + C \cdot \left(e^{D\frac{N}{1000}} - 1\right) \quad (8)$$

$$A = a_1 \cdot \left(\frac{\sigma_1}{\sigma_{1,f}}\right)^{a_2} \quad (8a) \qquad B = b_1 \cdot \left(\frac{\sigma_1}{\sigma_{1,f}}\right)^{b_2} \quad (8b)$$

$$C = c_1 \cdot \left(\frac{\sigma_1}{\sigma_{1,f}}\right)^{c_2} \quad (8c) \qquad D = d_1 \cdot \left(\frac{\sigma_1}{\sigma_{1,f}}\right)^{d_2} \quad (8d)$$

The model coefficients and r^2 – values as found for this model on the measured data by means of multi-variable non-linear regression analysis are given in Table 5. For each material the model has been used to describe both the axial and the radial strains, therefor in Table 5 two sets of model coefficients (axial and radial) are given for each material. For the ε_p-tests at D.o.C. = 103% a poorer fit is found for the model (lower r^2) than for ε_p-tests at D.o.C. = 97 and 100%. A close look at Figure 8 reveals that this is caused by the fact that the initial permanent strain (upto $N = 10^4$) is larger for the specimen tested at $\sigma_1/\sigma_{1,f} = 0.45$ than the specimen tested at $\sigma_1/\sigma_{1,f} = 0.52$. This is caused by variation between supposedly identical specimens resulting from specimen preparation. It has e.g. been observed that a slightly non horizontal top surface of the specimen causing the load to be applied not truly vertically results in accelerated accumulation of permanent strain.
Below a short breakdown is given of the various parts there are to the model.

The first part of the model:

$$\varepsilon_P = A \cdot \left(\frac{N}{1000}\right)^B$$

describes a "linear" increase of ε_p with N on a log(ε_p)-log(N) scales, where A then gives the ε_p at N = 1000 ("initial" permanent strain) and B gives the subsequent slope / increase of ε_p with N. Both A and B are of course stress dependent. The higher the vertical cyclic stress or stress ratio the higher both the initial strain and the increase of strain. The stress dependency of A and B is related (exponentially) to the $\sigma_1/\sigma_{1,f}$- ratio (equations 8a and 8b).
Material AL-40 at a D.O.C. of 97% typically shows this type of ε_p behaviour, which can therefor be perfectly described by only the first part (A and B) of the model. By fixing the values of c_1 (and d_1) to 0 the model simplifies to only the first part (see footnotes to Table 5).
From Figure 7 (and to a lesser extent Figure 8) it can be observed that material AL-40 at a D.O.C. of 100% (103%) for $N > 10^5$ and for the highest $\sigma_1/\sigma_{1,f}$–ratio does not show the "linear" but an "exponential " increase of ε_p with N on the same log(ε_p)-log(N) scales. The second part of the model:

$$..... + C \cdot \left(e^{d\frac{N}{1000}} - 1\right)$$

is able to describe such an "accelerated" increase.
This part of the model is able to describe, through the values of the regression coefficients (c_1 to d_2), at which value of N and at which value of the $\sigma_1/\sigma_{1,f}$ –ratio the "accelerated" increase takes place.

In the regression analysis it has been found that the solution of the stress dependency of C and D, i.e. the values for c_1-c_2 and d_1-d_2, can be indeterminate (various very different combinations of c_1-c_2 and d_1-d_2, give equal regression fits). It has therefor been decided to fix the values of c_1 and d_1 to 1 (see footnotes to Table 5).

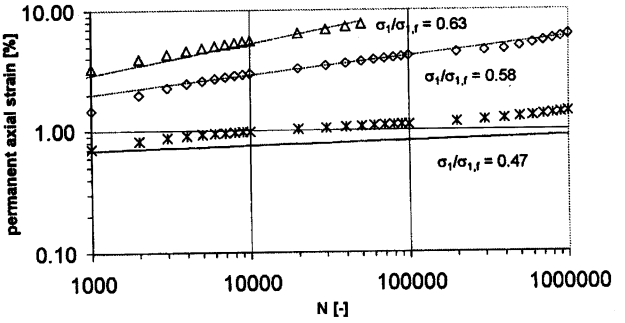

Figure 6: Permanent axial strain versus N for different stress levels (data and model) for AL-40 at a D.O.C. of 97%.

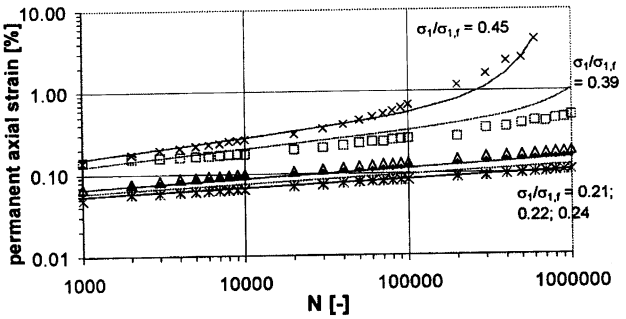

Figure 7: Permanent axial strain versus N for different stress levels (data and model) for AL-40 at a D.O.C. of 100%.

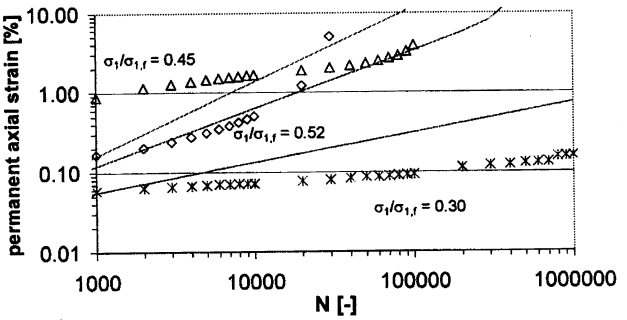

Figure 8: Permanent axial strain versus N for different stress levels (data and model) for AL-40 at a D.O.C. of 103%.

Although the $\sigma_1/\sigma_{1,f}$- ratio describes very well the stress dependency of ε_p in the model used here (equation 8) one has to make an interpretation step when comparing the different D.o.C. and/or materials. From e.g. Figure 6 and Figure 7 it can be seen that the $\sigma_1/\sigma_{1,f}$- ratios to which AL-97% has been loaded (0.47, 0.58 and 0.63) are higher than those for AL-100% (0.22, 0.39 and 0.45). At first glance this seems odd, one however has to realise that in terms of an *absolute* stress (σ_1) a lower $\sigma_1/\sigma_{1,f}$-ratio for AL-100% can ofcourse result in a higher σ_1 value because of the higher values of c and ϕ for AL-100% than those for AL-97% (Table 4).

Table 5. Model coefficients and r^2 – values as found for the ε_p-N-$\sigma_1/\sigma_{1,f}$–model on AL-40 at a D.O.C. of 97%, 100% and 103%

Material		a_1[1]	a_2	b_1	b_2	c_1[2]	c_2[3]	d_1[2]	d_2[3]	r^2
		[%]	[-]	[-]	[-]	[-]	[-]	[-]	[-]	[-]
sub-base	axial	-3.530	9.590	0.760	27.800	0	1	0	1	0.800
	radial	4.200	14.890	0.900	25.440	0	1	0	1	0.950
AL-97%	axial	-28.071	4.942	5.518	6.623	0	1	0	1	0.957
	radial	43.086	5.994	13.119	8.648	0	1	0	1	0.954
AL-100%	axial	-0.433	1.331	0.629	1.196	1	2.939	1	6.487	0.939
	radial	0.196	0.800	1.000	1.330	1	2.400	1	6.800	0.956
AL-103%	axial	-0.566	1.952	2.818	1.696	1	7.000	1	5.040	0.649
	radial	1.797	2.606	2.608	1.733	1	7.000	1	5.000	0.787

1: the following sign convention has been followed for strains:
- negative sign (-) for axial shortening and radial shrinking of the specimen
- positive sign (+) for axial and radial expansion of the specimen

2: for an in-active second part of the model c_1 and d_1 have been set to 0 and c_2 and d_2 have been set to 1

3: for an activated second part of the model c_1 and d_1 have been set to 1 and c_2 and d_2 are variable (the outcome of the regression analysis

To demonstrate this in Figure 9 the modelled development of $\varepsilon_p = f(N)$ at different *absolute* stress levels (σ_1=90, 135 and 180 kPa) is given for AL-97%, AL-100% and AL-103%. This has been calculated on the basis of the regression values for the model (equation 8) given in Table 5 and on the c and ϕ values given in Table 4. The ε_p –values in this figure are completely in line with what one would expect for the different D.o.C. levels, e.g. at σ_1=90 kPa AL-97% already shows considerable ep (8%) at N=103, while at σ_1=90 kPa AL-100% and AL-103% show negligible ε_p (<0.5%) at N=10^6. The apparent reversal between AL-103% and AL-100% at σ_1=135 and 180 kPa results from the fact that the measured ε_p data for Al-103% where on the basis of the 3 tests difficult to fit (see Figure 8 and the lower r^2-values, Table 5).

Figure 6, Figure 7 and Figure 8 demonstrate that the range of the $\sigma_1/\sigma_{1,f}$- ratio over which the material experiences either negligible or little ε_p or excessive ε_p is narrow. For AL-100% (Figure 7)

$\varepsilon_p < 1\%$ at $N=10^6$ for $\sigma_1/\sigma_{1,f} \leq 0.39$ while $\varepsilon_p < 8\%$ at $N=106$ for $\sigma_1/\sigma_{1,f} = 0.45$. For these tested base materials the $\sigma_1/\sigma_{1,f}$- ratio should also not exceed 0.5 – 0.6, to limit permanent deformation.
Earlier research on sub-base sands [Huurman, 1997] has demonstrated that for sands such a narrow range also applies but that such a threshold for the $\sigma_1/\sigma_{1,f}$- ratio lies *relatively* (much lower c and ϕ) higher 0.9-0.95.

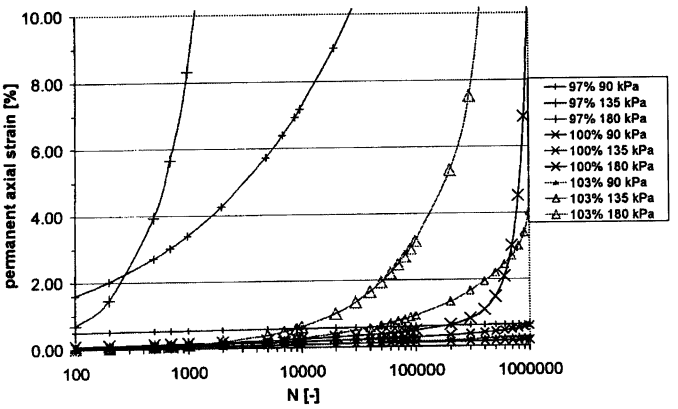

Figure 9: Development of $\varepsilon_p = f(N)$ at different absolute stress levels (σ_1=90, 135 and 180 kPa) (points only included to aid recognition – not specific data points)

4 Finite element analyses

To demonstrate influence of the D.o.C. of these base course materials on the actual performance of pavements finite element analyses (FEM) have been conducted based on the measured material behaviour described in section 3.
These analyses integrate the overall influence of the D.o.C. on the different types of material behaviour (failure, resilient and permanent deformation behaviour).
To take account of the stress dependent (non-linear) material behaviour the calculations have been made by means of FE-analysis rather than using (non-) linear elastic multi layer analysis.
To demonstrate the influence of the D.o.C. of the base course in different types of pavements, the analyses have been performed for a concrete block (CB) and two asphaltic (HMA) toplayers.
The FEM used is NOLIP [Huurman, 1997], a non-linear axial symmetric programme capable of accurately modelling:

- the discontinuous nature of a CB toplayer or a linear elastic toplayer (HMA, concrete),
- non-linear stress-strain behaviour for granular material layers, by means of various non-linear material models.

The limited length of this paper does not allow to go into much detail on the characteristics of the programme, for more information the reader is referred to [Huurman, 1997].
Below very briefly some characteristics (layer thicknesses and constitutive models / stress-strain behaviour) of the analysed pavements are presented.

Layer thicknesses:

- HMA: h=50 mm and 100 mm, CB: h=80 mm (the toplayer thicknesses have been limited to provide pavement examples where the base course provides a considerable structural contribution to the pavement performance),
- base course: 300 mm
- sub-base: 500 mm
- subgrade: 16000 mm

Stress-strain behaviour of the pavement layers:

- HMA: linear elastic deformation behaviour E=7500 MPa, v=0.35
- CB: interaction between concrete blocks: joints modelled as normal and shear springs (spring stiffness: 5500 and 500 N/mm per mm joint width respectively), block rotation and translation possible, CB properties: E= 40.000 MPa, v=0.35.
- Base : AL-97%, 100%, 103%:
  - c and ϕ (Table 4),
  - from FE-analysis it has been found that a "stiffening" model as the M_r-θ model leads to attracting / concentration of (high) stresses in certain elements and very low stresses in adjacent elements, this is caused by the fact that in an iterative calculation an initially stressed (load centre) and thus stiffer element attracts stresses resulting in an increase of its stiffness, attracting even more stress and thus again increasing stiffness, etc. upto unrealistically high stress and stiffness values. A stiffness model should thus be able to "soften" to allow for redistribution of stresses between elements in a FEM. This is also in line with the behaviour observed in triaxial tests at higher (σ_d/σ_3-ratio's), as has been discussed section 3.2 . For the base and sub-base thus the following models have been used [Huurman, 1997]:

$$M_r = k_1\left(\frac{\theta}{\theta_0}\right)^{k_2} \cdot \left(1 - k_3\left(\frac{\sigma_1}{\sigma_{1,f}}\right)^{k_4}\right) \qquad (9)^1$$

  - Subgrade: has been modelled linearly elastic (E=50 MPa, v=0.49), which is acceptable as stresses in the subgrade ($z > 1$ m) are mainly the result of dead weight stresses rather than of traffic loading.

To model traffic loading by standard 100 kN equivalent axle loads, in such an axial symmetric FEM, a 50 kN equivalent single wheel load with a radius of 150 mm (σ = 0.707 MPa) has been applied. The 12 NOLIP calculations (3 toplayers x 4 D.o.C. of base) result in values for stresses (principal stresses and $\sigma_1/\sigma_{1,f}$-ratio's), strains and M_r (E) and v for each of the 576 elements of the mesh. This is the output of the so called "elastic calculation". On the basis of the $\sigma_1/\sigma_{1,f}$-ratio's out of the "elastic calculation", a program module calculates for each element the permanent axial and radial strains at incremental values for N (upto N=10^6) based on the appropriate ε_p-models for the base and the sub-base (from Table 5). The permanent deformation of the subgrade is calculated as $\varepsilon_p = \varepsilon_{el} \times 0.7\text{Log}(N)$, ε_{el} = elastic deformation of subgrade elements. By summation of the permanent strains of the elements over the depth of the mesh a rut depth profile at the pavement surface is obtained. The module takes lateral wander of the traffic into consideration. It is important to note that the calcu-

---

For the values of regression coefficients for AL-97%, 100%, 103% and 105% reference is made to [Muraya and van Niekerk, 2000]

lated rut depth originate from permanent deformation in only the granular layers (base, sub-base and subgrade), the module does at present not take permanent deformation in the asphalt layer into consideration (for the CB pavement this is of course not relevant as concrete blocks do themselves not experience permanent deformation).

To evaluate the performance of the analysed pavements the following design criteria have been considered:

1. allowable number of equivalent 100 kN axle load repetitions (N_{all}) for asphalt fatigue cracking an subgrade strain,
2. Shear failure ($\sigma_1/\sigma_{1,f}$-ratio) in granular layers (base and sub-base).
3. Rut depth at the pavement surface,

N_{all} has been calculated on the basis of:

- the horizontal tensile strain (et) at the bottom of the asphalt layer and the fatigue cracking criterion: $\log(N)= 33.50 - 7.36\log(S_{mix}) + 0.78.\log^2(S_{mix}) - 5.24\log(\varepsilon_t)$ [1]
- the vertical compressive strain (ec) at the top of the subgrade and subgrade permanent deformation criterion: $N = 6.15.10^{-7}.\varepsilon_c^{-4}$

ε_t and ε_c have been taken from the "elastic calculations" the fatigue cracking and permanent deformation criteria have been taken from the Shell Pavement Design Manual (SPDM, 1978).

As the subgrade is rather deep (> 800 mm) in these pavements Nall for asphalt fatigue cracking was found to be much more critical than N_{all} for subgrade permanent deformation. Figure 10 gives the N_{all} -values for the 50 mm and 100 mm asphalt pavements for the 4 D.o.C. Figure 10 shows that pavement life (N_{all}) increases by a factor of 8 to 16 by increasing asphalt thickness (h_{asf}) from 50 mm to 100 mm. And that the increase of the D.o.C. increases pavement life by a factor of 3.5 (h_{asf} = 50 mm) and 1.8 (h_{asf} = 100 mm).

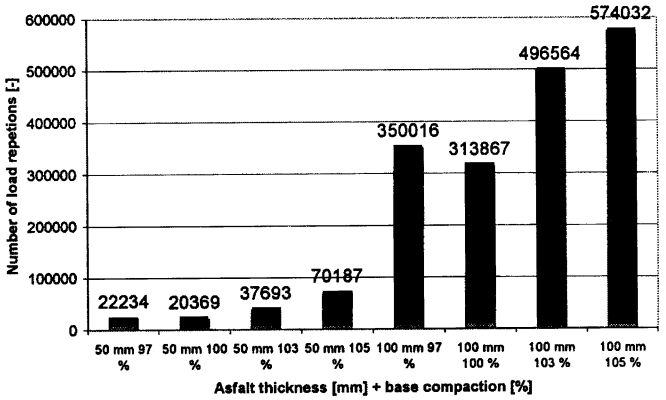

Figure 10: N_{all} for the 50 mm and 100 mm asphalt pavements for the 4 D.o.C.

---

[1] S_{mix} refers to the stiffness of the asphalt mix (in this analysis S_{mix}=7500 MPa)

From the "elastic calculations" the $\sigma_1/\sigma_{1,f}$–ratio of all elements in granular layers (base and sub-base) are obtained. A $\sigma_1/\sigma_{1,f} = 1$ would indicate shear failure under a single 50 kN equivalent single wheel load. High $\sigma_1/\sigma_{1,f}$–ratios indicate that excessive permanent deformation will occur under repeated loading. Figure 11, Figure 12 and Figure 13 give these $\sigma_1/\sigma_{1,f}$–ratios (at 240 mm from the central axis of the model) plotted against depth for the different D.o.C. for the 50 mm, 100 mm and the CB pavements, respectively.

Figure 11, Figure 12 and Figure 13 indicate that for all three pavement types the s$\sigma_1/\sigma_{1,f}$–ratio of the base decreases by a factor of 2 to 3 for an increase of D.o.C. from 97% to 105%. A close analysis of the "elastic calculations" shows higher M_r-values for the bases with higher D.o.C. resulting in higher stresses, but due to the higher c and f values for the higher D.o.C.(Table 4) $\sigma_1/\sigma_{1,f}$–ratios are still lower.

With respect to the sub-base for all pavements the increase of D.o.C. (increase of base stiffness) results in a slight reduction of the $\sigma_1/\sigma_{1,f}$–ratios in the sub-base.

Mutual comparison of these figures shows for all D.o.C. that the $\sigma_1/\sigma_{1,f}$–ratios of the base descend in relation to the toplayer type/thickness as follows 50 mm asphalt ⇒ CB ⇒ 100 mm asphalt. Indicating a better load spreading in a well constructed CB pavement then in a thin (50 mm) asphalt pavement and, of course, better load spreading in the 100 mm asphalt pavement than in the CB and the 50 mm asphalt pavement. With respect to the sub-base, the $\sigma_1/\sigma_{1,f}$–ratios of the sub-base ofcourse follow these same trends.

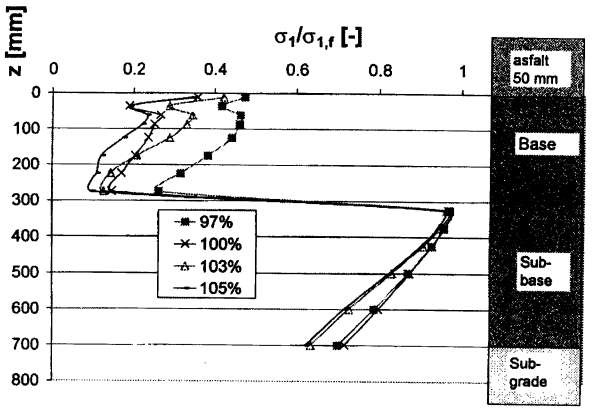

Figure 11: $\sigma_1/\sigma_{1,f}$–ratios in base and sub-base for D.o.C. 97%, 100%, 103% and 105% for the 50 mm asphalt pavement.

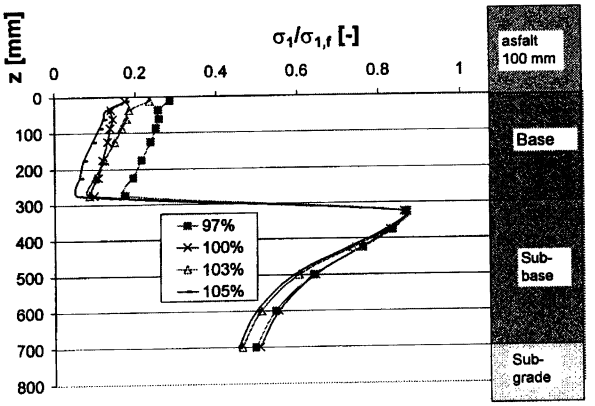

Figure 12: $\sigma_1/\sigma_{1,f}$–ratios in base and sub-base for D.o.C. 97%, 100%, 103% and 105% for the 100 mm asphalt pavement.

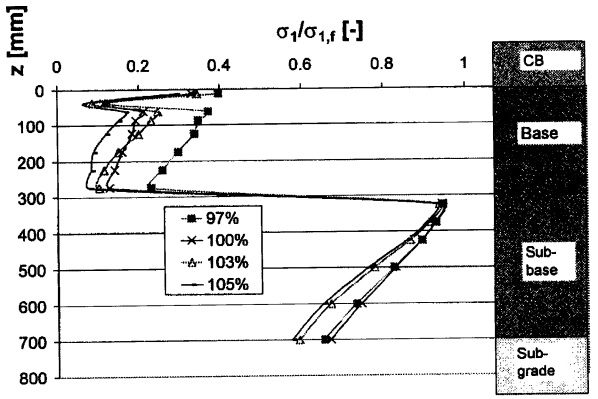

Figure 13: $\sigma_1/\sigma_{1,f}$–ratios in base and sub-base for D.o.C. 97%, 100%, 103% and 105% for the CB pavement.

From the calculated rut depth profiles as a function of N (see explanation on pg. 9) the absolute rut depth under a 1,20 m straight edge ($RD_{1,2m}$) has been calculated. In the Netherlands the performance criterion for rutting is $RD_{1,2m}$= 15 mm.

Figure 14, Figure 15 and Figure 16 show the rut depth as function of N for the 3 pavements for D.o.C. of the base of 97%, 100% and 103%, respectively. Each figure clearly shows the above discussed increase of load spreading (50 mm asphalt ⇒ CB ⇒ 100 mm asphalt) resulting in a reduction of $\sigma_1/\sigma_{1,f}$–ratios and thus of ε_p in the base and sub-base and as a consequence dramatic differences in rut depth. This is clearest for the pavements with a D.o.C. = 97% for the base coursebase course. For the 100 mm asphalt toplayer the $\sigma_1/\sigma_{1,f}$ –ratios in the base and sub-base are well below the "threshold" level and thus negligible rutting occurs (note that permanent deformation in the asphaltic layer is not taken into consideration). Under the 50 mm asphalt toplayer the $\sigma_1/\sigma_{1,f}$ –ratios

are considerably higher resulting in excessive rutting. The CB toplayer presents an intermediate case.

As $RD_{1,2m}$ is calculated from the rut depth profiles as the difference between the rutdepth in the central axis (RD_{0m}) and at 0.6 m ($RD_{0,6m\,(=1,2m/2)}$), $RD_{1,2m}$ can decrease in a step (from e.g. N=9000 to N=10.000) if in the specific step $\Delta RD_{0m} < \Delta RD_{0,6m}$. This explains the "bouncing" shape of some of the curves in Figure 14, Figure 15 and Figure 16.

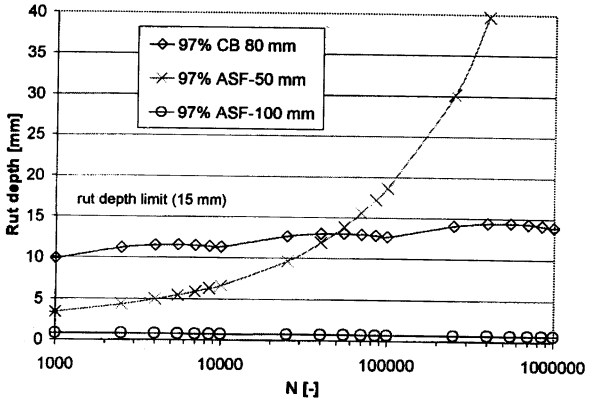

Figure 14: Rut depth as function of N for the CB, 50 mm and 100 mm asphalt pavements for D.o.C. = 97%

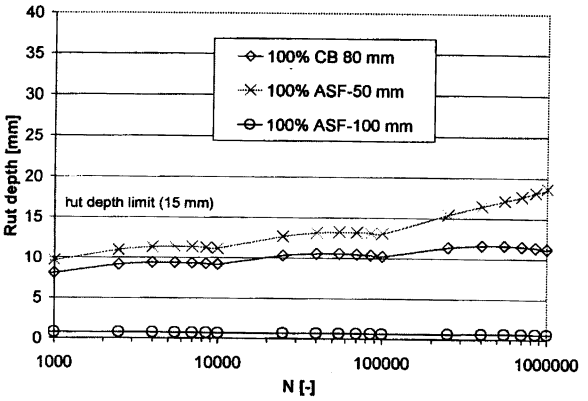

Figure 15: Rut depth as function of N for the CB, 50 mm and 100 mm asphalt pavements for D.o.C. = 100%

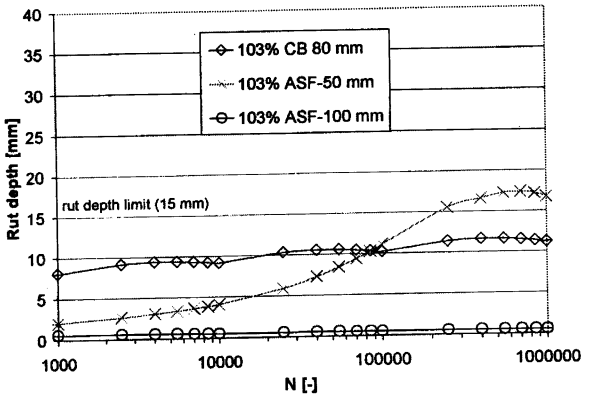

Figure 16: Rut depth as function of N for the CB, 50 mm and 100 mm asphalt pavements for D.o.C. = 103%

Figure 17 shows the rut depth as function of N for the 50 mm asphalt pavement for 97%, 100% and 103% D.o.C.[1] of the base. The figure clearly shows the difference between the pavements with on the one hand the "poorly compacted" 97% D.o.C. base which according to the 15 mm rut depth criterion has a pavement life of some N=75.10^3 and on the other hand the 100% and 103%[2] D.o.C. base which reach this criterion at N= 250.10^3. In addition the pavement with the 97% D.o.C. base shows a progressively increasing rut depth, while this rate clearly decreases for the 100% and 103% D.o.C. bases. When reaching its pavement life the "97%" pavement thus needs "immediate" reconstruction, while this can be "stretched" for the "100% and 103%" pavements.

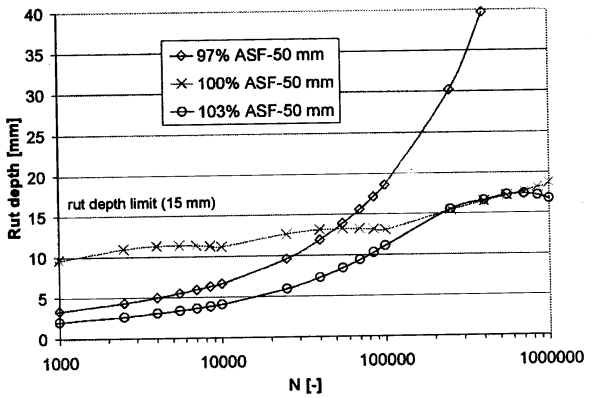

Figure 17: Rut depth as function of N for the 50 mm asphalt pavement for D.o.C. = 97, 100% and 103%

[1] the more or less similar rut depth development for $N \geq 1\ 10^5$, for the "100%" and the "103%" pavements results from the above explained poor fit of the permanent deformation model on the 103% D.o.C. tests.

[2] The "103%" shows a decreasing rut depth (RD) at $N \geq 8\ 10^5$, this should be understood as follows, the RD is calculated from the RD-profile as the relative RD under a 1,20 m straight edge ($RD_{1,2m}$=RD_0-$RD_{0.6m}$), at N ≥ 8.10^5 the increase of $RD_{0.6m}$ was found to be larger than the increase of RD_{0m}, resulting in $RD_{1,2m}$ at N= 9.10^5 to be slightly smaller than $RD_{1,2m}$ at N=8.10^5.

5 Conclusions

In this paper the influence of compaction on the mechanical behaviour of a granular base course material (mix granulate) and on the resulting performance of pavements is described. From the tri-axial tests performed to establish the mechanical behaviour of the investigated mix granulate at 4 levels of compaction and from the performed finite element calculations in which for three types of pavements only the degree of compaction (D.o.C.) of the base course has been taken as a design variable the following conclusions can be drawn.

With respect to the failure behaviour considerable increases of both the cohesion (c) and the angle of internal friction (ϕ) with increasing level of compaction have been observed. For an increase of the D.o.C. from 97% to 105% of MPD:

- c increases from 56 kPa to 142 kPa,
- ϕ: increases from 36.9 ° to 43.8 °.

With respect to the resilient deformation behaviour over the same range of D.o.C., the Mr-q relation shifts considerably, in terms of the Mr-values at levels of q of respectively, 100 and 800 kPa (Mr 100 and Mr 800), the following was observed:

- $M_{r\ 100}$ = 127 kPa (97% D.o.C.) and $M_{r\ 100}$ = 257 kPa (103% D.o.C.)
- $M_{r\ 800}$ = 284 kPa (97% D.o.C.) and $M_{r\ 100}$ = 571 kPa (103% D.o.C.)

The permanent deformation behaviour has been modelled by rather elaborate stress dependent models. If from these models permanent strains as a function of the number of load repetitions (N) are calculated at different absolute stress levels (s1) one observes that at a D.o.C. of:

- 97% for σ_1= 90 and 135 kPa some 10% permanent axial strain is reached at N=1500 and N=25000, respectively,
- 100% and 103% less 1% permanent axial strain is reached at N=106.

The above described influences of compaction on the mechanical behaviour were also observed in terms of predicted pavement performance using a F.E. model and the "Shell" performnace criteria. Pavement life in terms of the allowable number of equivalent 100 kN axle load repetitions (Nall) for asphalt fatigue cracking increased by a factor of 3.5 and 1.8 for the 50 mm and the 100 mm asphalt pavements, respectively, as the D.o.C. increased from 97% to 105%.

In terms of calculated rut depth the functional 15 mm rut depth criterion was reached for the 50 mm asphalt pavements at N=75.103 for 97% D.o.C., while for 100% and 103% D.o.C. this criterion was not reached until N= 250.103. Also beyond this criterion the 97% D.o.C. base showed a much more rapidly increasing rut depth with N than did the 100% and 103% D.o.C. bases.

Specification of an adequate level of compaction of the base course and tight control of the achieved compaction are considered to be amongst the most cost effective measures to increase pavement life for pavements in which a substantial structural contribution of the base course is required.

This research has also demonstrated that the combination of establishing fundamental material behaviour by means of triaxial testing and of finite element analysis of pavements based on such material behaviour, serves to sensibly predict and thus understand trends and mechanisms of various influence factors on pavement performance.

6 References

Brown, SF & Pell, PS, 1967, *An experimental investigation of the stresses, strains and deflections in a layered pavement structure subjected to dynamic loads*, Proc. 2nd Int. Conf. on the Design of Asphaltic Pavements, Ann Arbor, Michigan, U.S.

Centre R.O.W., 1995, *Standard R.A.W.-specifications* (in Dutch), Ede, The Netherlands.

Huurman, M, 1997, *Permanent deformation in concrete block pavements*, Ph.D. thesis, Delft University of Technology, the Netherlands.

Kisimbi, AJ & Niekerk, AA van, 1999, *Performance of mix granulate road bases in relation to mix composition and compaction*, M.Sc. thesis, Delft University of Technology, the Netherlands.

Niekerk, AA van, Scheers, J van & Galjaard, PJ, 2000, *Resilient deformation behaviour of coarse grained mix granulate base course materials from testing scaled gradings at smaller specimen sizes*, UNBAR 5.

Muraya, & Niekerk, AA van, 2000, *Permanent deformation behaviour in granular road bases*, M.Sc. thesis, Delft University of Technology, the Netherlands.

Sweere, GTH, 1990, *Unbound granular bases for roads*, Ph.D. thesis, Delft University of Technology, the Netherlands.

Uzan, J, Witczak MW, Schullion T & Lytton RL, 1992, *Development and validation of realistic pavement response models*, Proc. 7th Int. Conf. on the Structural Design of Asphalt Pavements, Nottingham, U.K., vol. 1, pp 334-350.